Accepted Manuscript

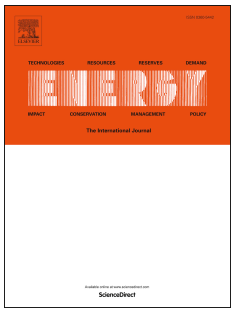

Power variability of tidal-stream energy and implications for electricity supply

Matt Lewis, James McNaughton, Concha Márquez-Dominguez, Grazia Todeschini, Michael Togneri, Ian Masters, Matthew Allmark, Tim Stallard, Simon Neill, Alice Goward-Brown, Peter Robins

PII: S0360-5442(19)31319-2

DOI: https://doi.org/10.1016/j.energy.2019.06.181

Reference: EGY 15664

To appear in: *Energy*

Received Date: 20 March 2019

Revised Date: 20 June 2019

Accepted Date: 29 June 2019

Please cite this article as: Lewis M, McNaughton J, Márquez-Dominguez C, Todeschini G, Togneri M, Masters I, Allmark M, Stallard T, Neill S, Goward-Brown A, Robins P, Power variability of tidal-stream energy and implications for electricity supply, *Energy* (2019), doi: https://doi.org/10.1016/j.energy.2019.06.181.

[1] Bangor University, UK
[2] Swansea University, UK
[3] Cardiff University, UK
[4] University of Oxford, UK
[5] Manchester University, UK

Abstract
Temporal variability in renewable energy presents a major challenge for electrical grid systems. Tides are considered predictable due to their regular periodicity; however, the persistence and quality of tidal-stream generated electricity is unknown. This paper is the first study that attempts to address this knowledge gap through direct measurements of rotor-shaft power and shore-side voltage from a 1MW, rated at grid-connection, tidal turbine (Orkney Islands, UK). Tidal asymmetry in turbulence parameters, flow speed and power variability were observed. Variability in the power at 0.5Hz, associated with the 10-minute running mean, was low (standard deviation 10–12% of rated power), with lower variability associated with higher flow speed and reduced turbulence intensity. Variability of shore-side measured voltage was well within acceptable levels (~0.3% at 0.5Hz). Variability in turbine power had <1% difference in energy yield calculation, even with a skewed power variability distribution. Finally, using a "t-location" distribution of observed fine-scale power variability, in combination with an idealised power curve, a synthetic power variability model reliably downscaled 30 minute tidal velocity simulations to power at 0.5Hz (R^2 = 85% and ~14% error). Therefore, the predictability and quality of tidal-stream energy may be undervalued in a future, high-penetration renewable energy, electricity grid.

Keywords: tidal energy, prediction, turbulence, power quality, Orkney, resource characterisation

1. Introduction

It is vital that countries convert to a sustainable low-carbon electricity system, and yet many renewable energy sources exhibit variability in power output over a range of time-scales with low predictability compared with traditional electricity sources (Drew et al. 2019). One of the key challenges integrating renewable energy into a guaranteed high-quality electricity supply is to ensure electricity supply matches demand (e.g. Barton and Infield 2004; Joos and Staffell 2018) – thus, reducing expensive storage and system control measures (Carrasco et al. 2006; Liserre et al. 2010; Milan et al. 2014).

There are many renewable energy sources, some of which are well established and dispatchable (e.g. hydro-electric and biomass), however recent interest in deploying a large amount of renewable energy sources (e.g. high penetration of renewable energy in a power grid) that are less dispatchable (i.e. the resource, thus electricity, is not always present) is discussed in context to the immature/developing tidal-stream energy industry. Fine-scale variability in renewable energy supplies arise from, for example, the passing of clouds for solar PV and gustiness for wind energy; it is this renewable energy variability that this paper discusses in context to tidal-stream energy. The predictability of clouds and therefore the persistence of solar energy is considered low (Brouwer et al. 2014; Wan et al. 2015), whilst turbulent fluctuations in wind speed (which we experience as gusts) are known to directly affect wind energy generation through changing wind turbine rotor speed (Sun et al. 2003; Brouwer et al. 2014). The variability of tidal energy is often quoted as low in comparison to

renewable energy power (POSTnote 2014). Different solutions are available to mitigate this concern, for example: the use of 'spinning reserve' when demand exceeds generation, and curtailment of energy sources when generation exceeds demand – as well as more sophisticated control strategies (see Grotz, 2008; Swain et al. 2017; Pinson et al. 2017). Both of these solutions result in significant drawbacks: spinning reserves include devices such as diesel generators and, therefore, they are potentially polluting and costly. Curtailment of energy sources means a reduced income for the owners and may potentially discourage further investment in renewable resources. Energy storage may be an alternative solution; however, large-scale storage for power grids is presently not widely deployed. Therefore, as a result of the variability of renewable energy resources, higher costs are expected to be incurred in a future low-carbon electricity system (Slootweg et al. 2003; Albadi and El-Saadany 2010; Joos and Staffell 2018).

In addition to variability of electricity supply, the shift of generation from fossil-fuelled energy sources to renewable generation creates a concern in relation to system inertia. Inertia of a power system is defined as the ability of a system to oppose changes in frequency, due to the kinetic energy stored in the rotating masses in synchronous generators. In an AC system, any imbalance between electricity supply and demand, will result in a change to the frequency; for example, when electricity demand exceeds generation, the system frequency will decrease. As a result, utilities and transmission system operators are concerned that a continuous decrease in system inertia will compromise grid stability (e.g. maximum deviation of 1% is tolerated at a nominal frequency of 50 Hz in the UK). Renewable sources that are decoupled from the grid, by means of power converters (e.g. solar-PV), do not contribute to system inertia unless specific requirements are introduced. For example, in Germany and Denmark (e.g. Joos and Staffell, 2018; Pinson et al. 2017), wind energy is contributing to system inertia. Therefore, tidal energy could also contribute to regulation of electricity supply.

The periodicity of the tide allows accurate tidal predictions far into the future using harmonic analysis or ocean modelling techniques (e.g. Lewis et al. 2017). For hydrokinetic turbines, which are used in tidal-stream electricity generation, the power (*P*) depends on the cube of velocity of the current ($\overline{U}$) at the site, the density of the fluid (ρ), the swept rotor area (A) and its design or "efficiency" (Cp): $P = 0.5 * \rho * A * Cp * \overline{U}^3$ [Eq. 1]. Following linear wave theory for a semi-diurnal system (like the UK), the resource ($\overline{U}$) is above 50% of peak flow for 67% of the tidal cycle, with the timing of peak flow advances 25.2 minutes each tidal cycle. Therefore, tidal energy is often publicised as a predictable and "high-quality" renewable energy source (e.g. Lewis et al. 2015).

In strongly semi-diurnal systems, the largest tides of the fortnightly "spring-neap" cycle always occur at a similar time of day (see Robins et al. 2015), due to the interaction of the phase-locked solar constituent (S2) and the lunar constituent (M2). Furthermore, the progression of the tidal wave, as it travels around the UK coastline, means a phase difference in the timing of peak tidal electricity production along a coastline could be exploited (Hardisty, 2008); for example, three tidal power stations 120° out-of-phase to one another would produce a constant amount of power over a tidal cycle for regions with a suitable coastline (it is unknown if such tidal systems exists elsewhere in the world as research in this area is preliminary, see Neill et al. 2016b). The predictability of tidal power could therefore be advantageous for baseload electricity within the UK's national grid, because arrays of tidal-stream turbines could be strategically sited along a coastline to

resolved every 15 to 60 minutes. The turbulent closure schemes applied in such models do not resolve realistic turbulent fluctuations and, hence, tidal power fluctuations. Turbulence is the fluctuation of velocity (u') within a time-mean window ($\overline{U}$); thus velocity at a point in time (u_t) is expressed as $u_t = \overline{U} + u'$. Turbulence at highly energetic tidal-stream sites is known to be relatively high (Thomson et al. 2012); for example, between 12-13% turbulence intensity (TI) at turbine hub–height (Milne et al. 2013), with differences noted between the flood and ebb tidal phases and surface-wave enhanced turbulence effects (Togneri et al. 2017; Togneri and Masters 2015).

Turbulent loadings (e.g. Afgan et al. 2013; Blackmore et al. 2016) and turbulence effects on thrust and power efficiency (Nishino and Willden 2012), have rightly been a focus of research in tidal energy. However, as the industry moves towards commercialization and the deployment of grid-connected devices (Magagna and Uihlein 2015), understanding the fine-scale current speed variability (i.e. turbulence) effects on electricity quality is therefore required; for both the development of the industry and integration of renewable energy at both national and micro-grid scales. Turbulence intensity at wind energy sites has been measured between 10% and 20% (Barthelmie et al. 2005; Barthelmie et al. 2007; Burton et al. 2011; Brown et al. 2013) and, therefore, wind turbulence is hypothesized to be slightly higher than turbulence at tidal energy sites (Hay et al. 2013; Hay 2018). The combination of slightly lower turbulence intensities at tidal-energy sites than wind sites, with the density of sea-water being ~800 times larger than air (see Eq. 1), suggests that fine-scale variability of tidal-stream energy should be lower than wind energy.

This paper aims to characterize tidal-stream power variability and develop a method that can downscale resource model information to efficiently predict electricity production for system operators. Using a unique 1 MW tidal-stream turbine data set, described in Section 2, we analyzed the variability of electricity and power within a running-average time window (Section 3). Our results (Section 4) present the first characterization of the quality of tidal-stream generated electricity, together with a method to downscale broad-scale (30 minute resolution) model data to predict electricity production at 0.5 Hz frequency. Hence, we communicate the value of tidal-stream energy in both micro-grid and national-grid renewable electricity systems (Section 5).

2. Case study and data

The tidal-stream energy resource of Orkney (UK) is one of the largest worldwide, recognized by the development of the European Marine Energy Centre (EMEC) full-scale tidal test site – where the tidal-stream energy device analysed in this study was located. The region has been extensively studied (e.g. Goward-Brown et al. 2017), and a number of models exist for the region; for example, that of Neill et al. (2014b) which will be applied in Section 4. The tidal wave takes around 2.5 hours to propagate in a clockwise direction around the Orkney Islands, which generates a strong pressure gradient flow through the Pentland Firth and the Firths of Orkney - tidal straits which link the Eastern-north Atlantic to the North Sea (see Figure 1). Tidal currents in the Firths of Orkney exceed 3 m/s in many locations, with water depths also suitable for the first generation of tidal turbine developments (Goward Brown et al. 2017); see Figure 1.

GE Renewable Energy's (formally Tidal Generation Ltd) 18 m diameter 1 MW turbine, DEEP-Gen IV, was deployed as part of the ETI funded ReDAPT project, in the Fall of Warness at the EMEC site (see Figure 1). Real time generator power (measured behind the generator within the nacelle) and shore side voltage (measured after the shore

Further details of the data are given in McNaughton (2015) and Ahmed et al. (2017) and flow data is available via the University of Edinburgh's data share (http://redapt.eng.ed.ac.uk) - see Sellar and Sutherland (2016).

Data was provided by GE and has been normalised to protect commercial sensitivity. Therefore, figures are presented in this publication as percentages relative to 20% above the stated capacity (i.e. maximum power of device, Pr, in order to ensure a 1 MW rated power at the shore connection) and rated velocity (Ur), when the instantaneous velocity (u_t) is predicted to provide instantaneous power (P_t) at the rated turbine capacity ($P_t = Pr$). Therefore, all data is presented as a percentage relative to the value at rated power: this means we express velocity and power respectively as $\left({u_t}/{Ur}\right) \times 100\%$ and $\left({P_t}/{Pr}\right) \times 100\%$.

3. Method and Preliminary Analysis

All time-series data were linearly interpolated to a common time-series at a frequency of 0.5 Hz. Some uncertainty in the synchronicity of data-series (of the order of seconds) was noted (e.g. McNaughton 2015), but this will not affect our analysis as we explore variability from a mean value within averaging windows of the order of minutes to hours. The interpolated 0.5Hz time-series of tidal-stream turbine power, shore-side voltage, and current velocity (at turbine hub height) allows an investigation into the fine-scale temporal variability of tidal-stream energy and potential causes (i.e. mean flow speed, turbulence and waves). Characterisation of the distribution of fine-scale turbine power variability, relative to the time-averaged mean (including sensitivity test to window choice), was performed. The fitted distribution of fine-scale turbine power variability allows a statistical method to down-scale tidal-stream hydrodynamic resource model information to fine-scale predictions of resource– which is presented in Section 4.

The 0.5 Hz (2 cycles per second) time-series of hub height tidal current velocity and tidal turbine shaft-power is shown in Figure 2. The fine-scale temporal variability of tidal current and power are highlighted in Figure 2, when compared with 30-minute running means (black line of Figure 2). The broader temporal variability of the resource appears to be accurately captured using hydrodynamic tidal resource models (e.g. Lewis et al. 2015), whilst the fine-scale variability of tidal-stream power is both novel and substantive (see Figures 2 and 3). The fine-scale variability of tidal-stream power is clearly shown in the power curve of Figure 3, comparing the 0.5 Hz measured power curve with an idealised power curve typically used in resource estimation and 30-minute hydrodynamic model data (e.g. Lewis et al. 2015). This fine-scale variability in tidal-stream energy, the focus of this study, is crucial to understand because it allows systems to be designed to ensure renewable electricity can be useful to end users. Moreover, the fine-scale variability of Figure 2 may be important for uncertainty quantification in resource estimation; thus, improving investor confidence in power curve estimation (Figure 3).

It should be noted how the idealised power curve (red line of Figure 3) is similar to the power observed at 0.5Hz, even though the idealised power curve is based on a different device deployed in a very different tidal environment (Strangford Lough, see Lewis et al. 2015) and applies 30-minute hydrodynamic model data for current speed (see Eq. 1). Therefore, broader-scale and turbulence scales of velocity fluctuations, and the subsequent power captured by the turbine, is the difference between the red line and the black dots of Figure 3. Finer-scale fluctuations in the 30-minute mean velocity (x-axis of Figure 3) clearly

above 100% were also recorded in Figure 3, due to the device rating being associated with the shoreside power rather than the turbine rotor shaft power, and hence much data at ~95% power above rated velocity.

Averaged spectra of the 0.5 Hz data are presented using Fast Fourier Transform (FFT) in Figure 4, with power and velocity normalised. These are obtained by computing separate spectra for each hour-long subset of the data record, with a half-hour overlap between subsets and applying a Hann window to prevent aliasing. Although this FFT analysis has limitations, the effect of waves in oceanographic data such as this is routinely analysed with FFT (e.g. Lewis et al. 2019) and a clear mode of oscillation is present in Figure 4 during a large wave event: There is no significant periodicity to the fine-scale variability with the exception of the October time-series: the peak visible in both the velocity (panel a) and power (panel c) around 10s (10^{-1} Hz) coincides with a large wave event. Wave data was taken from the ERA interim hindcast data (see Dee et al. 2011) for the corresponding model cell, and indicates a daily averaged offshore significant wave height of ~7 m and mean period of ~10 s for the 26-Oct-14. The apparent effect of waves to power is interesting, and Figure 4 implies that the turbine has been able to extract some additional energy from the presence of waves, but quantifying this effect is beyond the scope of this paper.

To test the sensitivity of our analysis to the choice of averaging window, a Kolmogorov-Smirnov test (KS) for goodness of fit (see Massey 1951) was applied with the null hypothesis (H) that the two data-series groups come from the same distribution (giving an associated P value of confidence in the result). No difference in our results was found when using sub-hourly time-averaging windows: see Table 1. Therefore, based on the results of Table 1, we find the variability in flood and ebb tidal power significantly different, but the October and November dates can be grouped together for analysis if a running mean, of the order of minutes, is used.

Differences in the power curve with various moving-average windows, and the associated error (difference in the sum of power in the two tidal cycles between the 0.5 Hz and the time-averaged power time-series), is shown in Figure 5. The results of Table 1 and Figure 5, along with previous studies of turbulence intensity quantification at tidal-stream energy sites (Milne et al. 2013), voltage variability (Larsson 2002; MacEnri et al. 2013) and fine-scale wind-power variability (Albadi and El-Saadany 2010), led to a 10 minute moving average window being used for analysis in our study (which averages out any wave influenced oscillations) - with data grouped for flood and ebb tides.

The variability of power, relative to the 10-min mean (δP), is also expressed as a percentage relative to the mean ($\delta power$) so the distribution of power variability relative to a time-averaging window can also be achieved. This variability in observed power, relative to the time-averaging window ($\delta power$), has units of percentage relative to the mean (which will therefore be zero, whilst $\delta power$ can be negative) see Eq. 2: $\delta power = \frac{\sigma}{\bar{P}} \times 100\%$ [Eq. 2]. Whilst the standard deviation of power within the time-mean window is expressed in units of percentage relative to rated power, the power variability ($\delta power$) is important for downscaling resource ocean model information to 0.5 Hz power. All power data was therefore included in the distribution of power variability, including outliers when no power was recorded even above rated speed (see Figure 2 and 3), because a realistic

and associated standard deviation (σ) of turbulence fluctuations (u') within the moving average window using Eq. 3: $TI = \frac{\sigma}{\bar{U}} \times 100\%$ [Eq. 3]. The major impact of energy variability on power quality is in relation to the deviation of voltage from the rated value – this will be referred to as 'voltage variability' in the paper. Voltage variability (F) was calculated as normalised root mean squared error associated with the running-mean shoreside measured voltage ($\bar{V}$) and associated variability ($V_t - \bar{V}$) of the shoreside measured voltage; see Eq. 4 (where b = a+10 mins and n is record length) in line with previous studies of relative voltage change (Larsson 2002; MacEnri et al. 2013): $F = \left(\left(\frac{\sum_{t=a}^{t=b} (V_t - \bar{V})^2}{n} \right) \div \bar{V} \right) \times 100$ [Eq. 4].

4. Results

Using a 10 minute moving average on the 0.5 Hz data, the mean tidal current and associated turbulence intensity (Eq. 3), as well as turbine measured power and voltage variability (Eq. 4) was calculated; see Figure 6 and Figure 7 for 26-Oct-2014 and 26-Nov-2014, respectively. The Kolmogorov-Smirnov test (KS) for goodness of fit results (Table 1) indicate the data of the two tidal cycles (Oct and Nov) are similar (at 5% signficance level), but significant flood/ebb assymetry is present in both tidal current and turbine power(Figures 6 and 7). FFT analysis of the 0.5 Hz data (Figure 4) suggests varibility in power around ~10 seconds, potentially due to waves and with slightly higher TI values in October (Figure 6), the effect is removed with the time-averaging window and hence the similiarity test result of Table 1.

In both Figures 6 and 7 the ebb tide appears first in the time series (the conditions between zero hours and ~6 hours). The ebb tidal condition has comparatively larger associated current speeds than the flooding tide in both dates; with larger broad-scale varibility features in the flooding tide (see black line of 10-minute moving average) and slightly higher turbulence intensity (TI) values, which is shown in Table 2. No strong linear correlation between voltage variability (F), mean flow speed or TI was found ($R^2 < 9\%$), with the flood and ebb mean F values at ~0.3% (Table 2). A voltage variation below 3% at 1 Hz or 0.3% at 8.8 Hz is defined as "tolerable" (MacEnri et al. 2013), which interpolating this to 2 second data suggests a tolerable level of less than 2.4% voltage variation. Furthermore, although some higher F values can be seen in Figures 6 and 7, all F values are well below that defined as "tolerable".

The hypothesised correlation between current speed variability (defined here as Turbulence Intensity, TI) and the variability in tidal turbine power produced is explored further in Figure 8, with the linear correlation statistics detailed in Table 3. The strong relationship between mean flow speed, TI and variability of tidal turbine produced power ($\delta power$), within the 10-minute running mean, can be clearly seen in Figure 8d. Power variability ($\delta power$) was found to decrease with increasing mean flow speed (Figure 8a), largely because it is a percentage of the variability around the mean value and the mean power increases with flow speed. However, the more pronounced effect (based on the flood-ebb distributions in Table 1) of decreasing power variability with increasing flow speed (and decreasing TI) on the ebb tides (gradient, m, of Table 3) appears to drive the significant differences of the fine-scale power variability between the flood and ebb data (R^2 values in Table 3). Further, power variability ($\delta power$) was found to increase with increasing levels of TI, as shown in Figure 8c and largely because TI decreases with increasing mean flow speeds (Figure 8b); hence the relationship shown in Figure 8d and described in Table 3.

respect to mean flow speed (U as a percentage of rated velocity) and TI. The result of the multiple regression is shown in Equations 5 and 6, with an associated R^2 of 71% and 77% for flood and ebb tides respectively:

$$\delta power\ (flood) = 34.90 - 0.38\overline{U} + 0.52TI + 0.02(\overline{U} \times TI) \quad [Eq.5]$$

$$\delta power\ (ebb) = -42.87 + 0.25\overline{U} + 9.19TI - 0.05(\overline{U} \times TI) \quad [Eq.6]$$

Not all variability was captured with a multiple linear regression (Eq. 5 and Eq. 6, and Figure 8d), potentially due to turbine behaviour and flow characteristics being measured at the turbine hub-height (instead of the entire turbine swept area) - as well as a likely phase lag between observed flow variations and power produced by the turbine. Another method is therefore required to resolve the fine-scale variability to enable synthetic power production models for energy system design. Instead, we explored the distribution of power variability (with respect to the 10-min mean power) to understand how to cascade resource hydrodynamic model information into fine-scale predictions of electricity production. Indeed, bias in the distribution of power variability must be present because there is a clear reduction in the net power over the two tidal cycles when using a running average window on the 0.5 Hz normalised power; as shown in Figure 5c.

The variability of power relative to the 10-min mean (δP) and the distribution of power varibility within the 10-min running mean of the 2 second data is shown in Figure 9. The distribution of the fine-scale variability of power clearly becomes more leptokurtic (sharply peaked) with increasing flow speeds in Figure 9; for both flood and ebb tidal conditions the power fluctuations become less compared to the mean. However, the shape of the distribution in power variability appears to change in Figure 9, which is important to understand for bias correction in resource assessment (e.g. see Figure 5c). Characterisation of the relative power variability distribution will allow a synthetic power production model to be used to represent fine-scale tidal power variability; hence hydrodynamic resource model output (typical outputs of 30 to 60 minutes) could be downscaled to predicted power at 0.5 Hz (of potential use to system operators).

The distribution of tidal velocity and tidal turbine power in Figure 10 shows interesting trends when grouped (data grouped between flood and ebb tides – and for tidal current speeds: below turbine cut-in speed (i.e. U is ~30% of rated U), between cut-in and rated velocity, and above rated velocity). Velocity variance, relative to the time-averaged 10-minute mean ($\bar{x}$) (Figure 10a and 10b), was normally distributed, matching a normalised Gaussian distribution described by Eq. 7 (where σ is standard deviation): $y = \frac{1}{\sigma\sqrt{2\pi}}\, e^{-\frac{x-\bar{x}}{2\sigma^2}}$ [Eq. 7]. The power variability (relative to the 10-minute mean power) is not normally distributed (see Figure 10 and Table 4); hence, there is an over-estimation of energy if we do not include the effects of turbulent fluctuation on power (see Figure 5c) and the discretised distribution of fine-scale power variability (see Figure 9). The negatively skewed (S) distribution of the power variability is shown in Figure 11 and Table 4, alongside the Kurtosis (K) of the distribution.

Figure 11 shows how the variability (e.g. standard deviation, σ in Fig. 11b) of normalised power increases with tidal current speed (U), becoming more negatively skewed (Figure 11c) with increasing Kurtosis values (Figure 11d); indicating normalised power variability distributions are asymmetric, with heavier distribution-tails and sharper peaks as velocity increases – especially pronounced in Ebbing tide data (shown in Figure 10) when voltage variability (F) is slightly higher and yet the turbulence intensity is lower (Figure 7 and 8). The result of the power variability distributions in Table 4 (using the Lilliefors test, with a

in Eq. 8, with the gamma function (Γ) and parameters of shape (υ), scale (ϑ) and location (μ); shown in Table 4 (as these parameters, which describe the distribution's shape, vary with current speed):

$$y = \frac{\Gamma\left(\frac{\upsilon+1}{2}\right)}{\sqrt{\upsilon\pi}\Gamma\left(\frac{\upsilon}{2}\right)}\left[\frac{\upsilon+\left(\frac{x-\mu}{\vartheta}\right)^2}{\upsilon}\right]^{-\left(\frac{\upsilon+1}{2}\right)} \quad \text{[Eq. 8]}.$$

Applying this *t location scale* distribution (Eq. 8), with the shape (υ), scale (ϑ) and location (μ) parameters (shown in Table 4, and Figure 12 for finer discretisation of velocity groups, i.e. 10% U groups), allows synthetic power to be generated using low temporal resolution velocity data. Therefore, a fine-scale tidal-stream turbine power time-series can be generated using low resolution tidal current data (i.e. from a hydrodynamic resource model), which can be used for electrical system and grid integration analysis. To demonstrate this synthetic power production model, a realistic fine-scale tidal power time-series (at 2 seconds) was generated using tidal velocity data output from a hydrodynamic tidal-resource model (of Neill et al. 2014b) at a frequency of 30 minutes, and the idealised power curve presented by Lewis et al. (2015) - see Figure 3.

The synthesised fine-scale power model is compared to that measured for the 26-Nov-2014 data in Figure 13. Although the 30 minute hydrodynamic model tidal velocity data has none of the characteristics of the tidal-stream energy device (apart from cut-in and rated power values; see Figure 3), the distribution of fine-scale power are similar; as shown in the "QQ" (quantile-quantile) plot of Figure 13.d, which shows the two distributions are similar (at the 5% significance level) with a KS test result of 0.03 (P value <0.01). Therefore, using a synthetic power production model (using *t location scale* distribution, with the shape (υ), scale (ϑ) and location (φ) parameters of Table 4, and in Figure 12), fine-scale realistic power can be predicted at 0.5 Hz based on 30 minute velocity data; an important step for grid-integration within electrical systems.

5. Discussion

Rapid fluctuations in power generated by renewable energy sources are known to cause problems to power system operation because they result in power unbalance and power quality issues (e.g. Ellis et al. 2015). Fine-scale variability of power from a tidal-stream turbine was observed for a site in Orkney (Figure 3). This variability is shown to have a bias, because there is a reduction in the net power in two tidal cycles when the averaging period is increased (Figure 5c). However, fine-scale power variability had only a small effect on resource estimates (Figure 5), with less than 1% error in the energy harvested by the tidal turbine for frequencies typical of resource modelling studies. Hence, a standardized device power curve can be applied to coarse hydrodynamic resource model data for accurate resource assessment without the need to include fine-scale resource variability (i.e. turbulence) or device characteristics (beyond swept area, cut-in and rated speed and power). Furthermore, fine-scale power variability (see Figure 3) can be statistically characterized, and downscaled, for electricity supply design strategies (Figure 13). Therefore, this study provides the first discussion of the power and elec bring produced by tidal-stream turbines which could be undervalued in the current renewable energy support stratergies.

A strong linear relationship was found between power variability, associated with a 10 minute running mean, and both turbulence intensity and mean flow speed (see Table 2). Power fine-scale varibility characteristics were consistent for a wide range of time-averaging

power was measured (Table 1), the observed fine-scale power variability was similar to that measured in other tidal turbines at different locations (e.g. Khan et al. 2008; MacEnri et al. 2013). Our observations of fine-scale turbine power variability were higher than those measured in a lower turbulence environment (see MacEnri et al. 2013; Thiringer et al. 2011), yet average TI values measured in our study were lower than those measured at another tidal-stream energy site (Milne et al. 2013; Togneri and Masters 2015): 9-12% compared to 12-13%.

Flood-ebb asymmetry was found in the tidal currents, with faster ebb current speeds and higher turbulence measurements (mean TI of ~9% during the ebb and 12% during the flood; Table 2), matching those simulated in the Fall of Warness by Neill et al. (2014b), and other sites (e.g. Milne et al. 2013; Togneri and Masters 2015). Fine-scale power variability was higher during the flood tide, likely because current speeds are lower then and power variability decreased with high current speeds (above rated velocity, when power capping also occurred; see Figures 9 - 11). Moreover, an oscillation in the mean current speed and power during the flooding tide was observed for both dates (Figure 6 and 7), which may also explain the increase in flood-tide power variability. This broad-scale oscillation feature of the flood tide was not predicted by the Neill et al. (2014b) model but could be caused by an eddy feature, perhaps generated by a neighboring bathymetric or topographic feature and then migrating through the site as it is sheds and persists (e.g. Neill et al. 2012). This variability in flow direction may be the cause of some recorded power variability, and future work ought to resolve current direction as well as magnitude. For example, zero power was recorded for some instances of high current speeds (Figure 2C and Figure 3), which may be due to changes in tidal current direction causing turbine blade stall, although this event occurred during a period of large waves and thus could be due to wave-tide interaction processes (see Lewis et al. 2014).

The Fast Fourier Transform (FFT) of tidal turbine power (Figure 4) produced similar results to those by Thiringer et al. (2011), with two exceptions: Firstly, the spectral peak associated with a ~10 second period, in both power (Figure 4a) and hub height current speed (Figure 4c) for the October data. Secondly, the temporal resolution of the power measurements in this study were not high enough to resolve the modes of power oscillation observed by Thiringer et al. (2011) below 2 seconds, which were potentially due to the turbine blade passing the support structure (Mason-Jones et al. 2013). The spectral peak within the October data coincided with a large wave event offshore of the site (based on ERA-interim data the 0.125° resolution re-analysis product; see Dee et al. 2011), and could be scope for future research as waves are known to affect the tidal resource (Lewis et al. 2014) and measurements of turbulence (Togneri et al. 2017). Indeed, the results of our power quality analysis may be considered location- and device-specific (e.g. rotor speed control mechanisms, such as pitch control, may differ between devices; Georgilakis 2008), and therefore further work is needed to assess the quality of tidal-stream electricity at a variety of sites in comparison to other forms of renewable energy. Further work is also needed to understand the effect of fine-scale tidal turbine power variability when aggregated to the power output from an array of devices (see MacEnri et al. 2013). For example, variability in wave energy is well known but can be mitigated by a number of spatially separated sites (Fairley et al. 2017).

The estimated tidal turbine voltage variability (F) matches that measured by MacEnri et al. (2013) for the SeaGen tidal device, with values within the limit defined as tolerable (no strong linear correlation between F, mean flow speed or TI was found, and mean F values

the higher predictability.

The power variability observed in this study agrees with Uihlein and Magagna (2016), who report the variability of tidal energy to be much better than other forms of renewable energy, such as wind (e.g. Potter and Negnevitsky 2006) and wave energy (e.g. Blavette et al. 2011; Kovaltcgouk et al. 2016). Indeed, storage mechanisms to mitigate the effects of renewable power variability (such as flywheel and batteries; e.g. Khan et al. 2011; Rahimi et al. 2013) can also be applied to tidal energy; for example, as tidal energy is surrounded by water, novel pumped-hydro (Rahimi et al. 2013) and hydrogen (Ren et al. 2017) storage solutions could be incorporated.

The characterization of tidal power variability, for storage solution design and optimization, is clearly an important research question that future studies should aim to resolve (e.g. the size of storage required for electricity users may not be large in comparison to other renewable forms). Indeed, tidal energy is considered one of the more expensive renewable electricity forms (Neill et al. 2018), and energy storage would increase costs further. Therefore tidal energy integration may appear less expensive when the costs of both technologies are included (i.e. Levelised Cost of Energy, storage and grid integration solutions) – especially within micro-grids with a high penetration of intermittent and less controllable renewable energy forms (for example, 100% renewable energy micro-grids for remote communities in fuel poverty)

Another method to mitigate the impact of fluctuations in renewable power supplied to the power grid, as well as design effective system control measures, is to accurately predict power variability. Methods of predicting power variability are well established in the wind industry, by using high-fidelity and computationally expensive Large Eddy Simulation (LES) models to simulate fine-scale wind field progression through a site, and thus predict fluctuations within the wind resource (e.g. Liu et al. 2011). Tidal energy is often stated to be predictable, due to the periodicity of the tide (e.g. Lewis et al. 2017), yet predictions of turbulent fluctuations in the tidal current would require similar LES methods. Another method of predicting fluctuations in the tidal energy resource could be established with a power variability probability density distribution, as has also been applied in the wind industry (e.g. Ellis et al. 2015).

In our study, tidal velocity characteristics did not fully, and directly, characterize the observed power variability (Table 2) – potentially as velocity measurements made at hub height cannot represent flow characteristics throughout the entire turbine swept area. Therefore not all variability observed in Figure 3 can be quantified due to instrument uncertainty and the lack of high-resolution flow data throughout the swept area of the turbine, which should be investigated in future studies; however the observed variability of measured power can be statistically characterized (Figure 10). Fine-scale power variability distributions enable a simple statistical prediction method for energy supplied by a wind turbine based on synoptic (i.e. mean flow) information (e.g. Rahimi et al. 2013; Ren et al. 2017), noted as computationally less expensive (e.g. Ellis et al. 2015), and allow comparisons of power quality to be made between wind and tidal turbines.

The tidal turbine power variability (shown in Figure 9 and 10) was found to be different to that of wind turbines. This variability can also clearly be seen in Figure 3, and the analysis of power variability in Figure 10 (~60%) finds the distribution is similar to that shown by Ren et al. (2017), but only the resource (current speed variability), not power, matched a

Fine-scale tidal turbine power variability was found to be well described by the *t location scale* distribution; where distributed velocity groups (x) in a probability distribution (y) are described in Eq. 8, with the gamma function (Γ) and parameters of shape (υ), scale (ϑ) and location (μ); shown in Table 4. Therefore, the likely tidal power at 0.5 Hz can now be predicted based on 30-minute-averaged current speeds output from an ocean model (or using a tidal prediction algorithm), together with knowledge of cut-in and rated velocity of the tidal turbine (the idealised power curve of Lewis et al. 2015 assumes a device efficiency, *Cp*, of 60% within Equation 1). When using the 30-minute hydrodynamic model simulations of Neill et al. (2014b) and an idealised power curve of Lewis et al. (2015), the fine-scale power variability model performed well (R^2 85% and RMSE of 14%, but with an energy difference of less than 0.7% for the tidal cycle), and produced a statistically similar distribution (see Figure 13) of power variability. Therefore, the variability observed in Figure 3 can be resolved, and coarse hydrodynamic resource model data can be statistically downscaled to provide accurate resource predictions, even at very high temporal resolution and with a idealised power curve based on a different tidal turbine (twin rotor MCT device – see Lewis et al. 2015). Considering the current high cost of tidal-stream energy, compared to other temporal variability renewable energy sources, the predictability of tidal-stream energy could be an asset in high penetration renewable energy distributed electricity supplies.

Future work could improve on the simple statistical model presented here (downscaling resource to 0.5 Hz power), by increasing the observational data and the dependency of fine-scale turbulent fluctuations (i.e. the temporal clustering of power variability). In the sampling of the statistical distribution, to downscale hydrodynamic model 30-minute data to 2 second power production, independence between data was assumed (i.e. a turbulent fluctuation synthesised at time *t* will not influence the next iteration at time *t*+*δt*). Future work should also aim to validate this fine-scale power prediction tool for different devices and sites, as well as exploring the use of power supply prediction in micro and national-scale grids to determine the true value of tidal power within a future renewable energy mix.

6. Conclusion:

The temporal variability and predictability of tidal-stream power was measured from a grid-connected 1 MW turbine in a highly energetic tidal site. For example, voltage variability was well within tolerable limits and no significant effect to estimates of annual mean energy yield were found (i.e. 1% reduction in energy calculated for typical resource assessment frequencies). Therefore, resource uncertainty due to fine-scale power variability appears low for tidal-stream energy, and idealised power curves (with accurate cut-in and rated flow speeds) are suitable for resource assessments – which we show can be statistically downscaled to fine-scale (2 Hz) power prediction. The value of tidal energy in power systems therefore appears to be undervalued, since this resource is perceived as being expensive (e.g. Levelized Cost Of Energy), without accounting for predictability. A skillful, yet simple, probability distribution model of power variability was applied to 30-minute hydrodynamic model data (tidal velocity at hub height) using the *t location scale* distribution, with parameters based on mean flow speed (which also described turbulence characteristics). Therefore, synthetic turbulence and fine-scale tidal turbine power variability model can be applied to low-temporal resolution resource data, with an idealised power curve, for a computationally efficient prediction of tidal-stream power.

7. Acknowledgements

Phil Coker from Reading University, UK for his useful comments and discussion. AGB wishes to acknowledge the financial support of the Welsh European Funding Office, and the European Regional Development Fund Convergence Programme. Data in this publication was allowed through a NDA and so is not publically accessible data. However, the hydrodynamic models and standardised method, applied throughout the publication, will allow replicability (because percentage change analysis was applied).

References:

Afgan, I., McNaughton, J., Rolfo, S., Apsley, D.D., Stallard, T. and Stansby, P., 2013. Turbulent flow and loading on a tidal stream turbine by LES and RANS. International Journal of Heat and Fluid Flow, 43, pp.96-108.

Ahmed, U., Apsley, D.D., Afgan, I., Stallard, T. and Stansby, P.K., 2017. Fluctuating loads on a tidal turbine due to velocity shear and turbulence: Comparison of CFD with field data. Renewable Energy, 112, pp.235-246.

Albadi M.H and El-Saadany E.F. 2010. Overview of wind power intermittency impacts on power systems. Electric Power Systems Research, 80. 627-632.

Barthelmie R, Hansen O, Enevoldsen K, Højstrup J, Larsen S, Frandsen S, Pryor S, Motta M, Sanderhoff P. Ten years of meteorological measurements for offshore wind farms. Journal of Solar Energy Engineering 2005; 127: 170–176.

Barthelmie, R.J., Frandsen, S.T., Nielsen, M.N., Pryor, S.C., Rethore, P.E. and Jørgensen, H.E., 2007. Modelling and measurements of power losses and turbulence intensity in wind turbine wakes at Middelgrunden offshore wind farm. Wind Energy: An International Journal for Progress and Applications in Wind Power Conversion Technology, 10(6), pp.517-528.

Barton, J.P. and Infield, D.G., 2004. Energy storage and its use with intermittent renewable energy. IEEE transactions on energy conversion, 19(2), pp.441-448.

Blackmore T, Myers L.E, Bahaj A.S. 2016. Effects of turbulence on tidal turbines: Implications to performance, blade loads and conditions monitoring. International Journal of Marine Energy, 14, 1-26.

Blavette, A., O'Sullivan, D.L., Lewis, A.W. and Egan, M.G., 2012, May. Impact of a wave farm on its local grid: Voltage limits, flicker level and power fluctuations. In OCEANS, 2012-Yeosu (pp. 1-9). IEEE.

Brouwer, A.S., Van Den Broek, M., Seebregts, A. and Faaij, A., 2014. Impacts of large-scale Intermittent Renewable Energy Sources on electricity systems, and how these can be modeled. Renewable and Sustainable Energy Reviews, 33, pp.443-466.

Brown, A.J.G., Neill, S.P. and Lewis, M.J., 2013. The influence of wind gustiness on estimating the wave power resource. *International Journal of Marine Energy*, *3*, pp.e1-e10.

Burton, T., Jenkins, N., Sharpe, D. and Bossanyi, E., 2011. Wind energy handbook. John Wiley & Sons.

Carrasco, J.M., Franquelo, L.G., Bialasiewicz, J.T., Galván, E., PortilloGuisado, R.C., Prats, M.M., León, J.I. and Moreno-Alfonso, N., 2006. Power-electronic systems for the grid integration of renewable energy sources: A survey. IEEE Transactions on industrial electronics, 53(4), pp.1002-1016.

Dee, D.P., Uppala, S.M., Simmons, A.J., Berrisford, P., Poli, P., Kobayashi, S., Andrae, U., Balmaseda, M.A., Balsamo, G., Bauer, D.P. and Bechtold, P., 2011. The ERA-Interim reanalysis: Configuration and performance of the data assimilation system. Quarterly Journal of the royal meteorological society, 137(656), pp.553-597).

Fairley I, H.C.M. Smith, B. Robertson, M. Abusara, I. Masters, Spatio-temporal variation in wave power and implications for electricity supply, Renewable Energy, *114*, pp.154-165.
Georgilakis, P.S., 2008. Technical challenges associated with the integration of wind power into power systems. Renewable and Sustainable Energy Reviews, 12(3), pp.852-863.
Grotz, C., 2008. The new Germany Renewable Energy Sources Act (EEG) and its impact on wind energy. *German Wind Energy Association (BWE) November*.
Goward Brown, A.J., Neill, S.P. and Lewis, M.J., 2017. Tidal energy extraction in three-dimensional ocean models. *Renewable energy*, *114*, pp.244-257.
Hay, A.E. 2018. Remote acoustic turbulence measurement in a high flow tidal channel. 2018 Australian Ocean Renewable Energy Symposium. 20-22 Nov. 2018
Hay, A.E., McMillan, J., Cheel, R. and Schillinger, D., 2013, September. Turbulence and drag in a high Reynolds number tidal passage targetted for in-stream tidal power. In Oceans-San Diego, 2013 (pp. 1-10). IEEE.
Hardisty, J., 2008. Power intermittency, redundancy and tidal phasing around the United Kingdom. *Geographical Journal*, *174*(1), pp.76-84.
Joos M., Staffell I., Short-term integration costs of variable renewable energy: Wind curtailment and balancing in Britain and Germany, Renewable and Sustainable Energy Reviews, 86, 2018, pp. 45-65,
Khan, J., Bhuyan, G., Moshref, A., Morison, K., Pease, J.H. and Gurney, J., 2008, July. Ocean wave and tidal current conversion technologies and their interaction with electrical networks. In Power and Energy Society General Meeting-Conversion and Delivery of Electrical Energy in the 21st Century, 2008 IEEE (pp. 1-8). IEEE.
Kovaltchouk, T., Armstrong, S., Blavette, A., Ahmed, H.B. and Multon, B., 2016. Wave farm flicker severity: Comparative analysis and solutions. Renewable Energy, 91, pp.32-39.
Larsson A. 2002. Flicker Emission of wind turbines during continuous operation. IEEE Transactions on Energy Conversion. 17(1), 114 – 118
Lewis, M., Neill, S.P., Robins, P., Hashemi, M.R. and Ward, S., 2017. Characteristics of the velocity profile at tidal-stream energy sites. *Renewable Energy*, *114*, pp.258-272.
Lewis, M., Neill, S.P., Robins, P.E. and Hashemi, M.R., 2015. Resource assessment for future generations of tidal-stream energy arrays. *Energy*, *83*, pp.403-415.
Lewis, M.J., Neill, S.P., Hashemi, M.R. and Reza, M., 2014. Realistic wave conditions and their influence on quantifying the tidal stream energy resource. *Applied Energy*, *136*, pp.495-508.
Lewis, M.J., Palmer, T., Hashemi, R., Robins, P., Saulter, A., Brown, J., Lewis, H. and Neill, S., 2019. Wave-tide interaction modulates nearshore wave height. *Ocean Dynamics*, *69*(3), pp.367-384.
Liserre, M., Sauter, T. and Hung, J.Y., 2010. Future energy systems: Integrating renewable energy sources into the smart power grid through industrial electronics. IEEE industrial electronics magazine, 4(1), pp.18-37.
Liu, Y., Warner, T., Liu, Y., Vincent, C., Wu, W., Mahoney, B., Swerdlin, S., Parks, K. and Boehnert, J., 2011. Simultaneous nested modeling from the synoptic scale to the LES scale for wind energy applications. Journal of Wind Engineering and Industrial Aerodynamics, 99(4), pp.308-319.
MacEnri J, Reed M, Thiringer T. 2013. Influence of tidal parameters on SeaGen flicker performance. Phil. Trans. Roy. Soc. A. 371: 20120247.
Magagna, D. and Uihlein, A., 2015. Ocean energy development in Europe: Current status and future perspectives. International Journal of Marine Energy, 11, pp.84-104.
Massey, F. J. "The Kolmogorov-Smirnov Test for Goodness of Fit." Journal of the American Statistical Association. Vol. 46, No. 253, 1951, pp. 68–78.

Milan P, Wachter M, Peinke J. 2014. Stochastic modelling and performance monitoring of wind farm power production. Journal of Renewable and Sustainable Energy, 6, 033119.

Milne I.A, Sharma R.N, Flay R.G.J, Bickerton S. 2013. Characteristics of the turbulence in the flow at a tidal stream power site. Phil. Trans. Roy. Soc. A. 371:20120196

Neill, SP, Jordan, JR & Couch, SJ 2012, 'Impact of tidal energy converter (TEC) arrays on the dynamics of headland sand banks' *Renewable Energy*, vol. 37, no. 1, pp. 387-397.

Neill, S.P., Hashemi, M.R. and Lewis, M.J., 2016. Tidal energy leasing and tidal phasing. Renewable Energy, 85, pp.580-587.

Neill, S.P., Cooper, M.M. & Lewis, M.J. (2016b) Global tidal phasing potential. 2016 Ocean Sciences Meeting, New Orleans, 21-26 February 2016.

Neill, S.P., Hashemi, M.R. and Lewis, M.J., 2014. Optimal phasing of the European tidal stream resource using the greedy algorithm with penalty function. *Energy*, *73*, pp.997-1006.

Neill SP, Hashemi MR, Lewis MJ. The role of tidal asymmetry in characterizing the tidal energy resource of Orkney. Renewable Energy. 2014b, Aug 1;68:337-50.

Neill, S.P., Angeloudis, A., Robins, P.E., Walkington, I., Ward, S.L., Masters, I., Lewis, M.J., Piano, M., Avdis, A., Piggott, M.D. and Aggidis, G., 2018. Tidal range energy resource and optimization–Past perspectives and future challenges. *Renewable energy*. 127, 763-778.

Nishino, T. and Willden, R.H., 2012. Effects of 3-D channel blockage and turbulent wake mixing on the limit of power extraction by tidal turbines. International Journal of Heat and Fluid Flow, 37, pp.123-135.

Olczak, A., Stallard, T., Feng, T. and Stansby, P.K., 2016. Comparison of a RANS blade element model for tidal turbine arrays with laboratory scale measurements of wake velocity and rotor thrust. Journal of Fluids and Structures, 64, pp.87-106.

Pinson, P., Mitridati, L., Ordoudis, C. and Ostergaard, J., 2017. Towards fully renewable energy systems: Experience and trends in Denmark. *CSEE journal of power and energy systems*, *3*(1), pp.26-35.

POSTnote 464, 2014, Intermittent Electricity Generation

Potter, C.W. and Negnevitsky, M., 2006. Very short-term wind forecasting for Tasmanian power generation. IEEE Transactions on Power Systems, 21(2), pp.965-972.

Rahimi, E., Rabiee, A., Aghaei, J., Muttaqi, K.M. and Nezhad, A.E., 2013. On the management of wind power intermittency. Renewable and Sustainable Energy Reviews, 28, pp.643-653.

Ren, G., Liu, J., Wan, J., Guo, Y. and Yu, D., 2017. Overview of wind power intermittency: Impacts, measurements, and mitigation solutions. Applied Energy, 204, pp.47-65.

Saqib, M.A. and Saleem, A.Z., 2015. Power-quality issues and the need for reactive-power compensation in the grid integration of wind power. Renewable and Sustainable Energy Reviews, 43, pp.51-64.

Sellar B.G. and Sutherland D R.J., 2016. Technical Report on Tidal Site Characterisation During the ReDAPT Project v4.0, 2016. Institute for Energy Systems, School of Engineering, University of Edinburgh

Slootweg J.G, Haan S.W.H, Polinder H, Kling W.L. 2003. General model for representing variable speed wind turbines in power system dynamics simulations. IEEE Transactions on power systems, 18 (1), 144-151.

Sun, T., Wang, W.S., Dai, H.Z. and Yang Y.H., 2003. Voltage fluctuation and flicker caused by wind power generation [J]. Power System Technology, 12, p.014.

Thomson J, Polagye B, Durgesh V, Richmond M. 2012. Measurements of turbulence at two tidal energy sites in Puget Sound, WA. IEEE Journal of Oceanic Engineering, 37, 363-373.Togneri, M., Lewis, M., Neill, S. and Masters, I., 2017. Comparison of ADCP observations and 3D model simulations of turbulence at a tidal energy site. Renewable Energy, 114, pp.273-282.

Togneri, M., Masters, I. 2015. Micrositing variability and mean flow scaling for marine turbulence in Ramsey Sound, Journal of Ocean Engineering and Marine Energy, (2015)

Wan, C., Zhao, J., Song, Y., Xu, Z., Lin, J. and Hu, Z., 2015. Photovoltaic and solar power forecasting for smart grid energy management. CSEE Journal of Power and Energy Systems, 1(4), pp.38-46.

TABLES:

Table 1. Similarity of distributions from grouped tidal-stream turbine data. The result of a two-sample Kolmogorov-Simrnov test (at 5% significance level); displayed as H (the result given as diff or same for the two groups tested), P (asymptotic p-value between 0 and 1), and KS (the test statistic as critical value).

		Velocity (various running means)					**Power (various running means)**				
Two groups tested		raw 2s data	10m mean	15m mean	30m mean	60m mean	raw 2s data	10m mean	15m mean	30m mean	60m mean
2 dates (all tides)	H	**diff**	**same**	**same**	**same**	**same**	**diff**	**same**	**same**	**same**	**same**
	P	0.00	1.00	1.00	1.00	1.00	0.00	1.00	1.00	1.00	1.00
	KS	0.05	0.00	0.00	0.00	0.00	0.06	0.00	0.00	0.00	0.00
Floods and ebbs	H	**diff**	**diff**	**diff**	**diff**	**diff**	**diff**	**diff**	**diff**	**same**	**diff**
	P	0.00	0.04	0.00	0.42	0.00	0.00	0.02	0.00	0.38	0.00
	KS	0.22	0.23	0.49	0.20	0.70	0.23	0.25	0.40	0.20	0.70
Floods: Oct and Nov	H	**diff**	**same**	**same**	**same**	**same**	**diff**	**same**	**same**	**same**	**same**
	P	0.00	1.00	1.00	1.00	1.00	0.00	1.00	1.00	1.00	1.00
	KS	0.1	0.00	0.00	0.00	0.00	0.12	0.00	0.00	0.00	0.00
Ebbs: between Oct and Nov	H	**diff**	**same**	**same**	**same**	**same**	**diff**	**same**	**same**	**same**	**same**
	P	0.00	1.00	1.00	1.00	1.00	0.00	1.00	1.00	1.00	1.00
	KS	0.05	0.00	0.00	0.00	0.00	0.09	0.00	0.00	0.00	0.00

Table 2. Mean values of variblity associated with two tidal cycles of tidal-stream turbine data, also split into flooding and ebbing tides: voltage variability, calculated using the varibility of 0.5 Hz measured voltage within a 10-min running mean (Eq. 4), and Turbulence Intensity, calculated using varibility within a 10-min running mean of the 0.5 Hz flow speed measured at hub height (Eq. 3).

	voltage variability (F)		Turbulence Intensity (TI)	
	flood	ebb	flood	Ebb
26-Oct-14	0.31%	0.33%	11.7%	11.3%

variability ($\delta\ power$ calculated from Eq. 2), for the tidal stream turbine power quality data described in Figure 7; when flow speed >35% rated. The gradient (m) and intercept (c) of the linear regression within form *y=mx+c* with associated R^2 value, and data grouped by date and tidal stage (flooding or ebbing tidal condition).

Data tested	Grouped data	Gradient (m)	Intercept (c)	R^2 (%)
$\delta\ power$ (y as %) and $\overline{U}$ (x as % rated) (Figure 8a)	floods Oct	-2.24	258	35
	flood Nov	-0.78	96	48
	ebbs Oct	-0.46	62	71
	ebbs Nov	-0.63	78	39
	Floods	**-0.39**	**55**	**63**
	Ebbs	**-0.75**	**95**	**43**
TI (y) and $\overline{U}$ (x) (Figure 8b)	floods Oct	-0.07	16	62
	flood Nov	-0.04	12	35
	ebbs Oct	-0.11	20	67
	ebbs Nov	-0.11	19	49
	Floods	**-0.05**	**14**	**43**
	Ebbs	**-0.10**	**19**	**50**
$\delta\ power$ (y) and TI (x) (Figure 8c)	floods Oct	30.87	-257	51
	flood Nov	3.68	-7	6
	ebbs Oct	22.77	-173	63
	ebbs Nov	6.66	-34	90
	Floods	**4.17**	**-17**	**54**
	Ebbs	**6.98**	**-38**	**75**

Table 4. The 10-minute probability distribution information of 0.5 Hz normalised tidal turbine power variability for two tidal cycles, and also grouped by tidal current speed, with velocity (U) below turbine cut-in speed (U<30% of rated velocity, when no power is produced), U between cut-in (30%) and rated turbine velocity (100%), and when current speeds are above rated velocity of the turbine (U>100%). The distribution that closest matches that observed is described and the KStest result given (with associated P-value), and the parameters required to describe this distribution given.

		Velocity (U)			Power (P)	
Grouped data result (based on velocity		U<30%	30%<U< 100%	U>100%	30%<U< 100%	U>100%
Flooding tide	Mean ($\bar{x}$)	-0.05	0.00	0.00	0.00	0.00
	S.D. (standard deviation, σ)	3.96	6.95	8.86	7.56	10.22
	Kurtosis (K)	3.09	3.43	3.12	6.07	4.16
	Skewness (S)	0.11	-0.10	-0.09	0.58	-0.90
	KStest result and p-value (in brackets)	0.01 (0.07)	0.01 (0.01)	0.01 (0.02)	0.11 (0.00)	0.16 (0.00)
	Closest distribution:	**normal**	**normal**	**normal**	**T-location**	**T-location**
	location (μ)	n/a	n/a	n/a	-0.26	2.09

	deviation, σ)	4.78	7.47	8.08	7.44	11.07
	Kurtosis (K)	3.41	3.53	3.46	5.41	14.87
	Skewness (S)	0.29	-0.07	-0.29	0.17	-1.58
Ebbing tide	KStest result and p-value (in brackets)	0.04 (0.00)	0.02 (0.00)	0.02 (0.00)	0.07 (0.00)	0.24 (0.00)
	Closest distribution:	**normal**	**normal**	**normal**	**T-location**	**T-location**
	location (μ)	n/a	n/a	n/a	-0.18	0.30
	scale (ϑ)	n/a	n/a	n/a	5.01	2.29
	shape (υ)	n/a	n/a	n/a	3.18	1.14

Figure Captions:

Figure 1. The location of the Fall of Warness in the Orkney Islands (panel a), in Scotland, UK (panel b) where the EMEC site is, and a grid-connected 1MW tidal-stream turbine was installed.

Figure 2. The 0.5 Hz hub height tidal current and tidal turbine power, normalised to the rated power conditions and with a 30 minute moving averaging (black line), for a tidal cycle in October 2014 (panel a and c) and November (panel b and d).

Figure 3. The normalised 0.5 Hz measured power curve for the two tidal cycles in 2014 compared to an idealised power curve (red line of Lewis et al. 2015) used in hydrodynamic model resource estimation.

Figure 4. Fast Fourier Transform analysis of the normalised and smoothed 0.5 Hz hub height tidal velocity (U) and turbine measured power (P) for two tidal cycles: one on 26-Oct-14 (panels a and c) and one 26-Nov-14 (panels b and d).

Figure 5. The observed variability of the 0.5 Hz measured power curve and various time-average windows (panel a). The standard deviation of the associated time-averaged power (P) and velocity (U) is shown in Panel b, and the associated error (as a percentage) in panel c: this shows the reduction in the sum of the power time-series using time-averaged data for the two tidal cycles compared to the 0.5 Hz data.

Figure 6. Tidal-stream power and turbine produced electricity quality for the 26-oct-2014 tidal cycle. The hub-height tidal current speed measured at 0.5 Hz, with the 10 minute moving average (black line) is shown in panel a. The associated turbulence intensity (TI) shown as a blue line in panel b, with tidal cycle average as a black line (flood and ebb means are dashed lines, with no disernable difference at this scale). The 0.5 Hz turbine measured power and 10 minute mean (black line) is shown in panel c. The shore-side measured voltage variability (V variability) shown as a red line in panel d, with tidal cycle average as black line, with flood and ebb mean values as dashed line.

(TI) shown as a blue line in panel b, with tidal cycle average as a black line (flood and ebb means are dashed lines, with no disernable difference at this scale). The 0.5 Hz turbine measured power and 10 minute mean (black line) is shown in panel c. The shore-side measured voltage variability) shown as a red line in panel d, with tidal cycle average as black line, with flood and ebb mean values as dashed line.

Figure 8. The relationship between 10-minute averaged tidal-stream turbine data and grouped by date (26-Oct-14 and 26-Nov-14) and flood (FD) or ebb (EB) tidal condition (see legend). Mean flow speed and 10-min tidal turbine power variability ($\delta power$ calculated from Eq. 2) shown in panel a; mean flow speed and Turbulence Intensity (TI calculated from Eq. 3) shown in panel b; power variability ($\delta power$) and TI shown in panel c. All 10-min data is shown in panel d as the relationship between power variability and TI, with mean flow speed shown as colours.

Figure 9. The probability distribution (coloured scale) of the relative (compared to the mean) variability of tidal-turbine power (δP), within a 10-minute moving average, compared to the flow speed, for the tidal turbine data of the 26-Oct-14 and 26-Nov-14 and grouped into flood (a) and ebb (b) and all (c) tidal conditions.

Figure 10. The probability distributions of the 10-minute running mean data grouped by flow seed conditions: (1) flow speeds less than cut-in speed of turbine (U<30% of rated speed); (2) flow speeds between cut-in and turbine rated speed (cut-in<U<100%); (3) flow speeds greater than turbine rated speed; shown as red, blue and black lines respectively with thin dashed lines connecting data points (circles) with the respective normal distribution (normalised) shown as thicker solid line. Flooding tide flow speed (panel a) and ebb tide flow speed (panel b) distributions are shown with respective turbine power distributions (panel c and d respectively), with the 10-minute running mean power curve show in in panel e.

Figure 11. The variability associated with the normalised 10-min moving window power average, measured at 0.5 Hz from a tidal turbine for two tidal cycles. The 10-min mean power curve for all data, and grouped into flooding and ebbing tides (panel a), with the standard deviation (S.D.), Skewness and Kurtosis of the power variability distributions in panels b, c and d respectively; and discretised to the nearest 10% velocity (U) group (based on rated tidal velocity of the turbine *i.e. when 10-min mean U is 100% of rated U).

Figure 12. the three parameters used to describe the t-location scale distribution of 0.5 Hz power, when using a 10-min moving average and normalising the power by rated velocity and the variability around the mean – grouped by flood and ebb tide for two tidal cycles (26-Nov and 26-Oct 2014), with data normalised by rated velocity and power.

power in panel b (with red line a 30-min moving average). Panel c shows the 30-minute hydrodynamic resource model power time-series (calculated using idealised power curve of Figure 2) and the synthesised 0.5 Hz power (grey; calculated applying the *t-location scale* distribution parameters of Figure 11), with the similarity of the 0.5 Hz synthesised power (P) and that observed (P) in panel d.

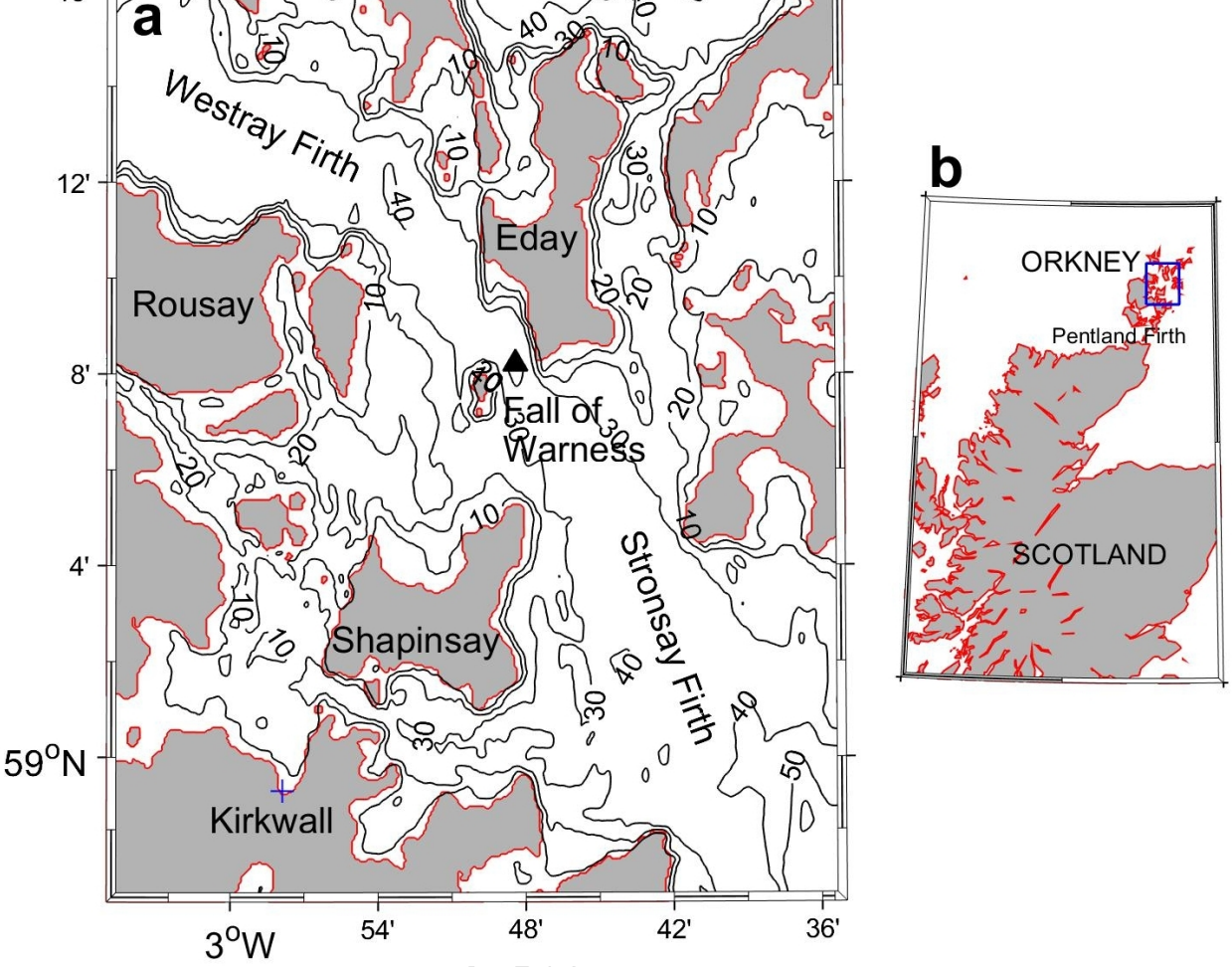
a
Westray Firth
Eday
Rousay
Fall of Warness
Shapinsay
Stronsay Firth
Kirkwall
12'
8'
4'
59°N
3°W
54'
48'
42'
36'
b
ORKNEY
Pentland Firth
SCOTLAND

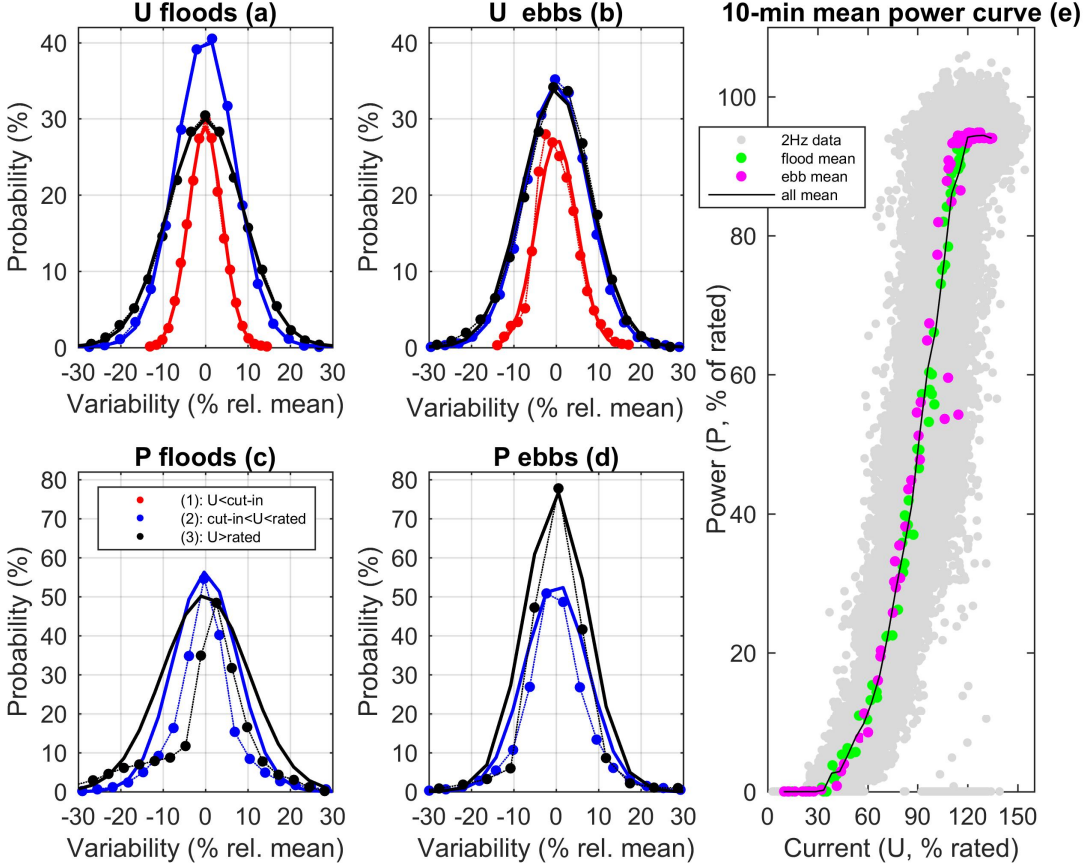
U floods (a)
U ebbs (b)
10-min mean power curve (e)
P floods (c)
P ebbs (d)
Probability (%)
Variability (% rel. mean)
Power (P, % of rated)
Current (U, % rated)
(1): U<cut-in
(2): cut-in<U<rated
(3): U>rated
2Hz data
flood mean
ebb mean
all mean

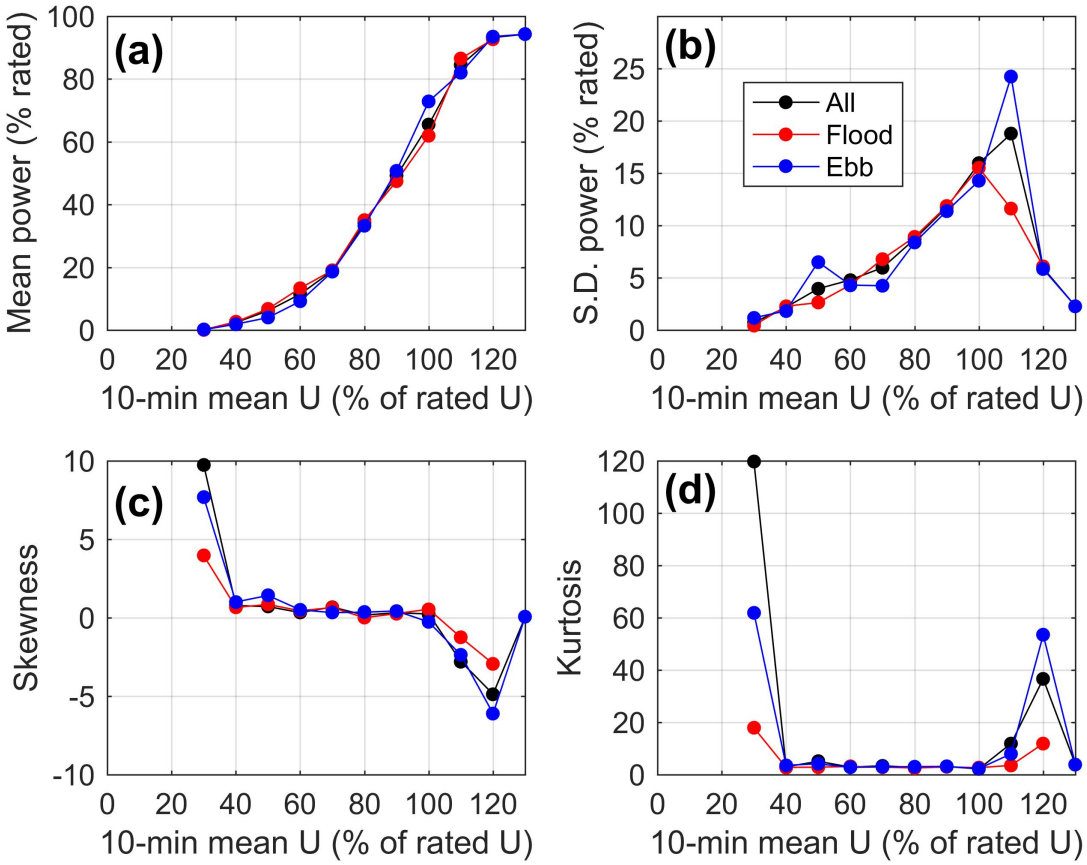
(a)
Mean power (% rated)
10-min mean U (% of rated U)
(b)
S.D. power (% rated)
All
Flood
Ebb
10-min mean U (% of rated U)
(c)
Skewness
10-min mean U (% of rated U)
(d)
Kurtosis
10-min mean U (% of rated U)

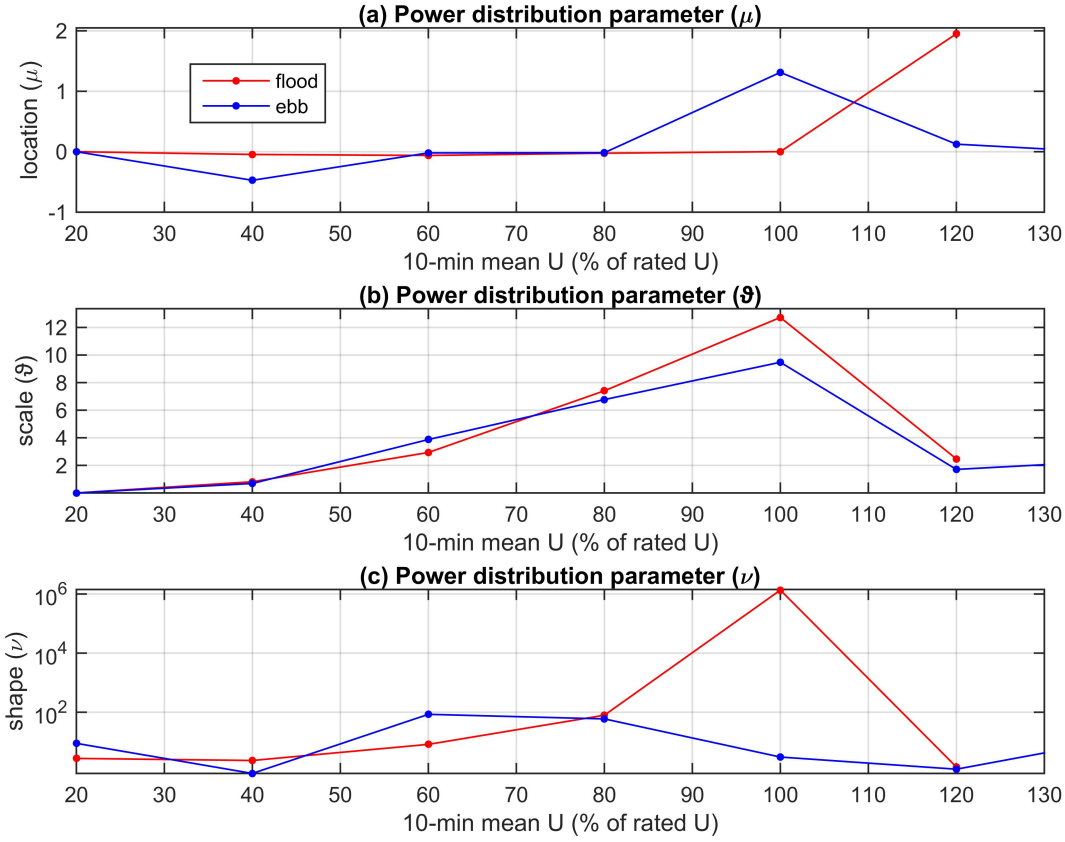
(a) Power distribution parameter (μ)
location (μ)
flood
ebb
10-min mean U (% of rated U)
(b) Power distribution parameter (ϑ)
scale (ϑ)
10-min mean U (% of rated U)
(c) Power distribution parameter (ν)
shape (ν)
10-min mean U (% of rated U)

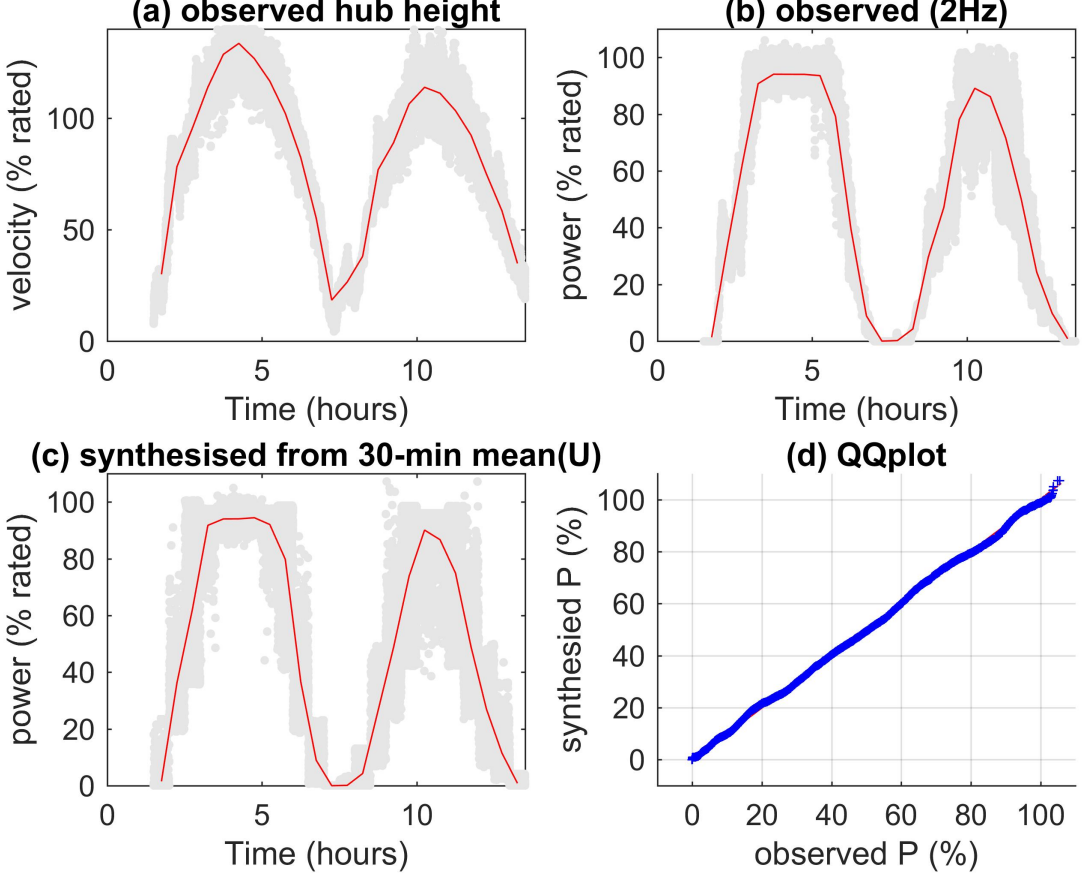
(a) observed hub height
velocity (% rated)
Time (hours)
(b) observed (2Hz)
power (% rated)
Time (hours)
(c) synthesised from 30-min mean(U)
power (% rated)
Time (hours)
(d) QQplot
synthesied P (%)
observed P (%)

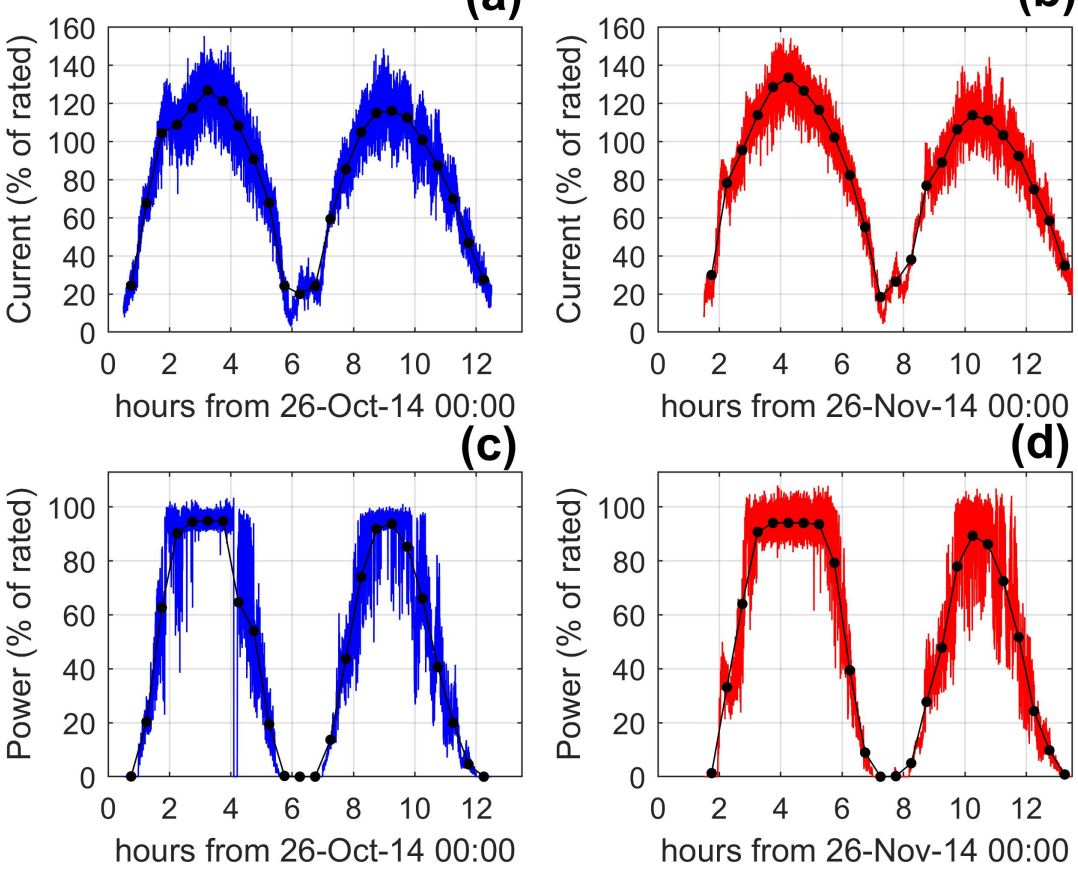
(a)
(b)
(c)
(d)
Current (% of rated)
Power (% of rated)
hours from 26-Oct-14 00:00
hours from 26-Nov-14 00:00

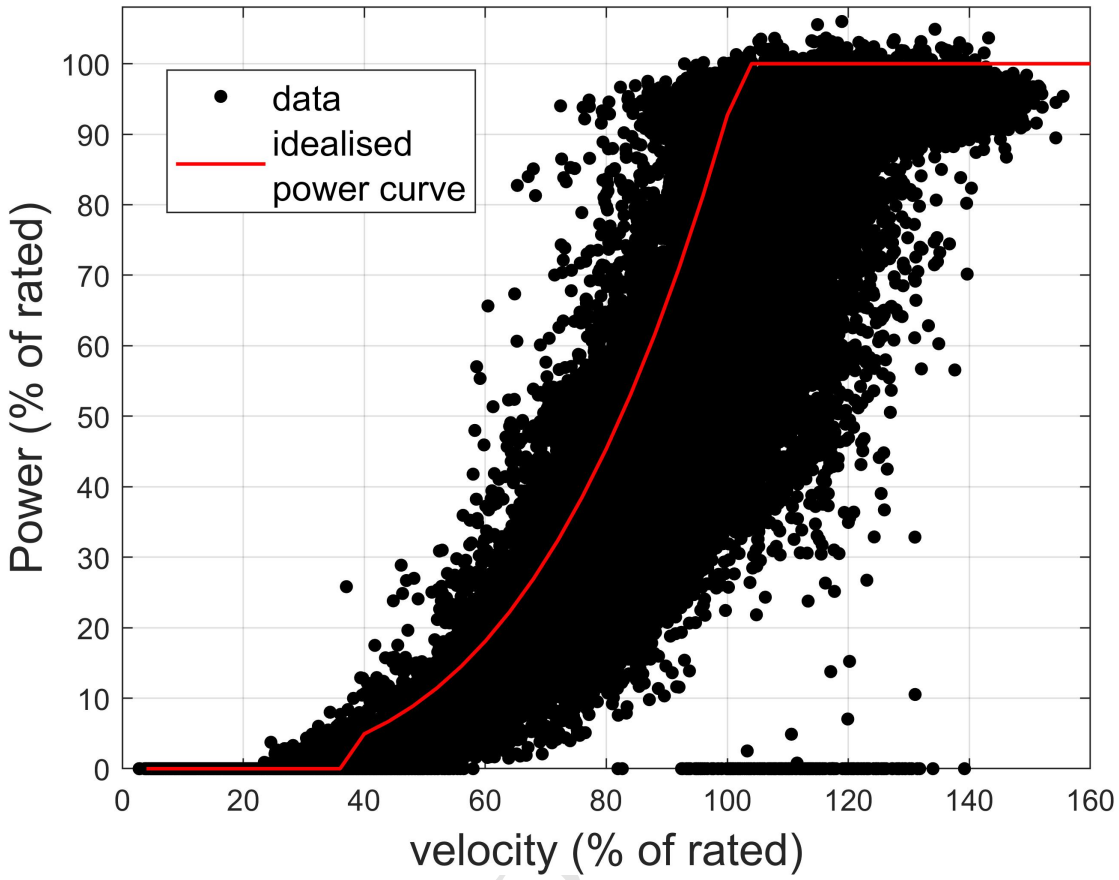
data
idealised
power curve
Power (% of rated)
velocity (% of rated)
0
10
20
30
40
50
60
70
80
90
100
0
20
40
60
80
100
120
140
160

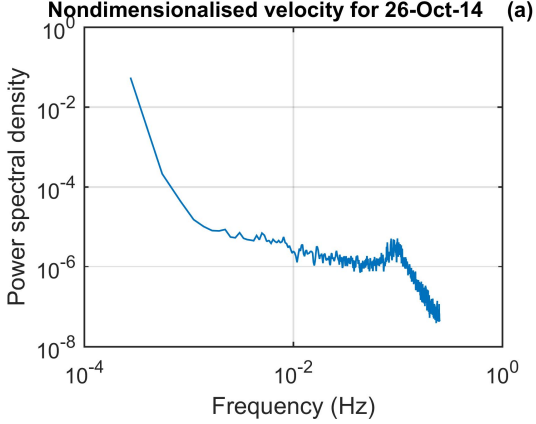
Nondimensionalised velocity for 26-Oct-14 (a)
Power spectral density
Frequency (Hz)

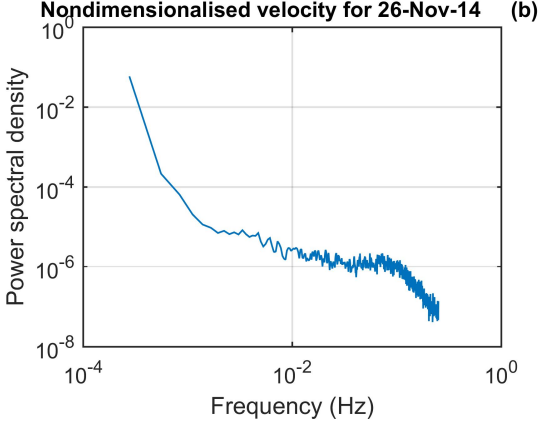
Nondimensionalised velocity for 26-Nov-14 (b)
Power spectral density
Frequency (Hz)

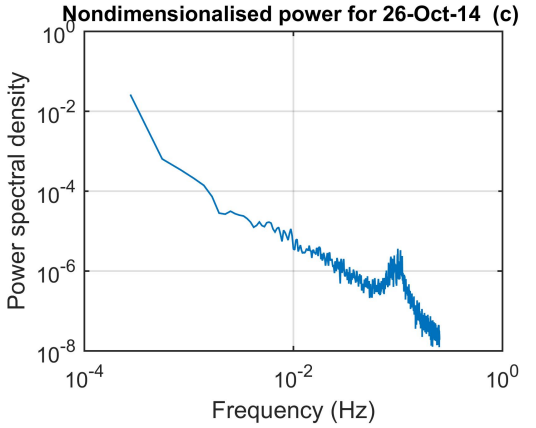
Nondimensionalised power for 26-Oct-14 (c)
Power spectral density
Frequency (Hz)

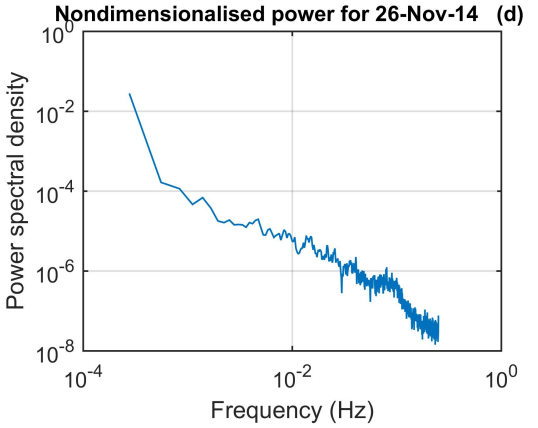
Nondimensionalised power for 26-Nov-14 (d)
Power spectral density
Frequency (Hz)

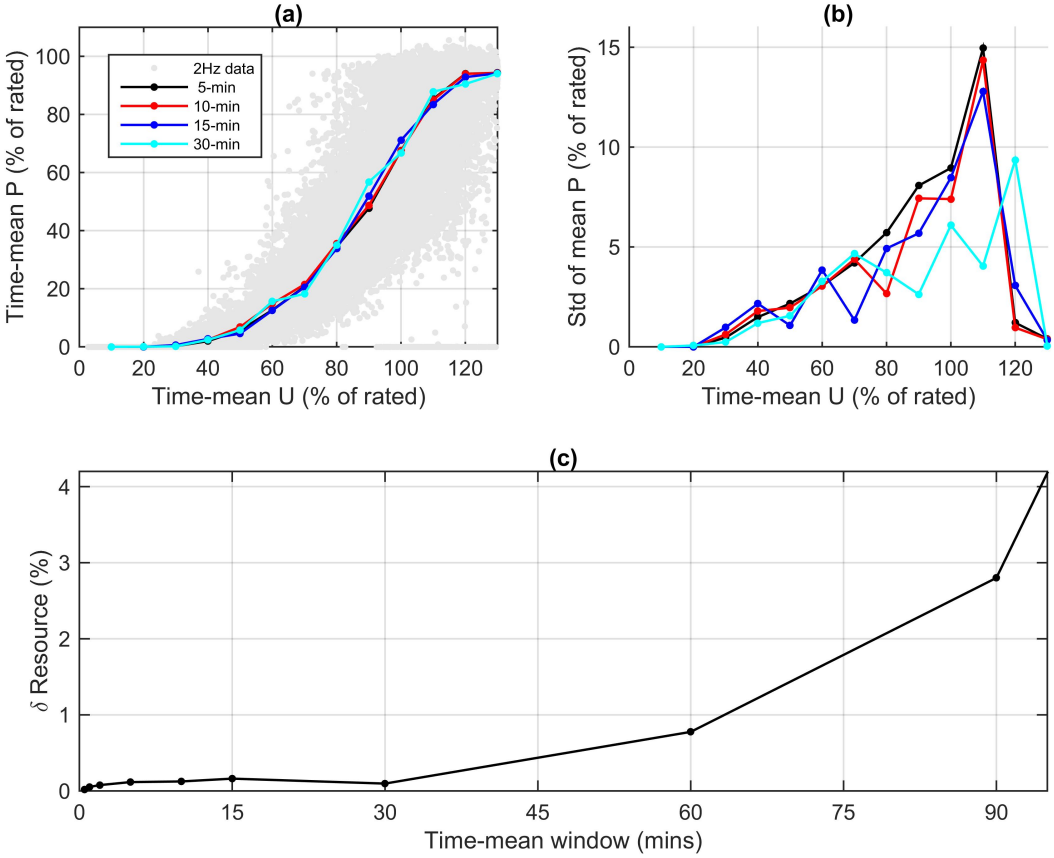
(a)
2Hz data
5-min
10-min
15-min
30-min
Time-mean P (% of rated)
Time-mean U (% of rated)
(b)
Std of mean P (% of rated)
Time-mean U (% of rated)
(c)
δ Resource (%)
Time-mean window (mins)

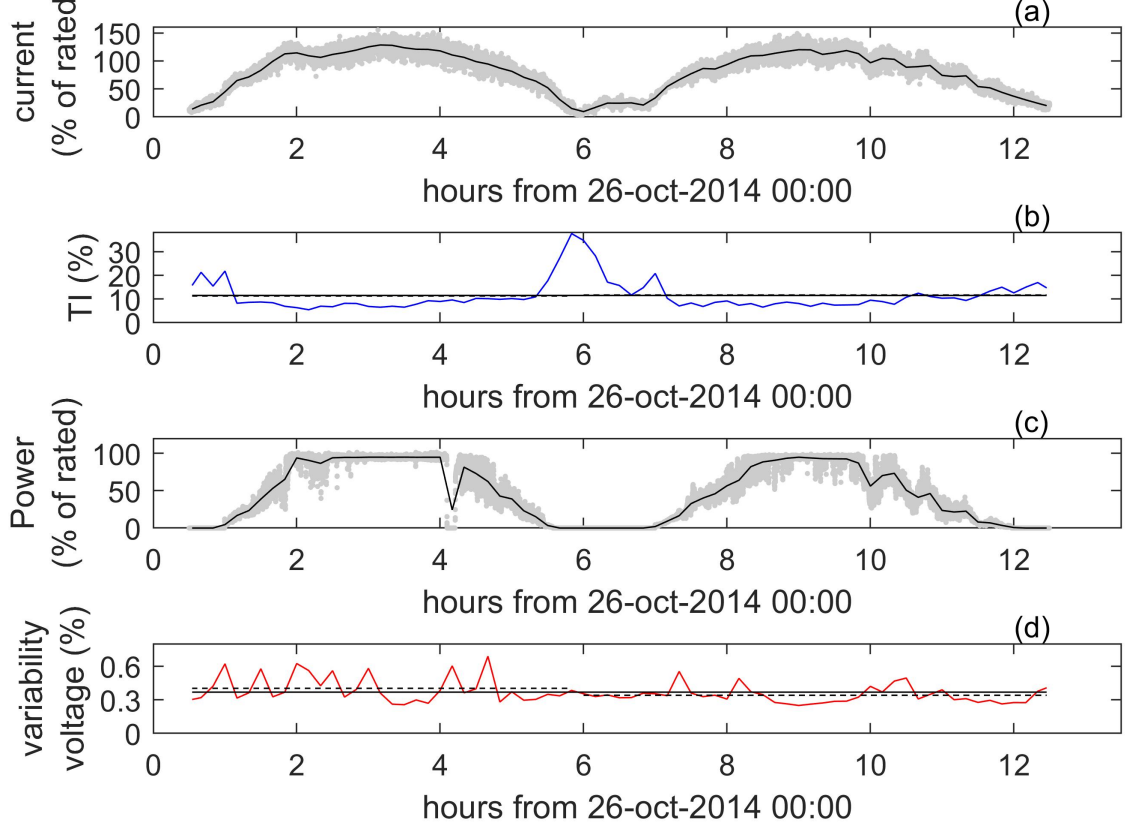
(a)
current (% of rated)
150
100
50
0
0
2
4
6
8
10
12
hours from 26-oct-2014 00:00
(b)
TI (%)
30
20
10
0
0
2
4
6
8
10
12
hours from 26-oct-2014 00:00
(c)
Power (% of rated)
100
50
0
0
2
4
6
8
10
12
hours from 26-oct-2014 00:00
(d)
variability voltage (%)
0.6
0.3
0
0
2
4
6
8
10
12
hours from 26-oct-2014 00:00

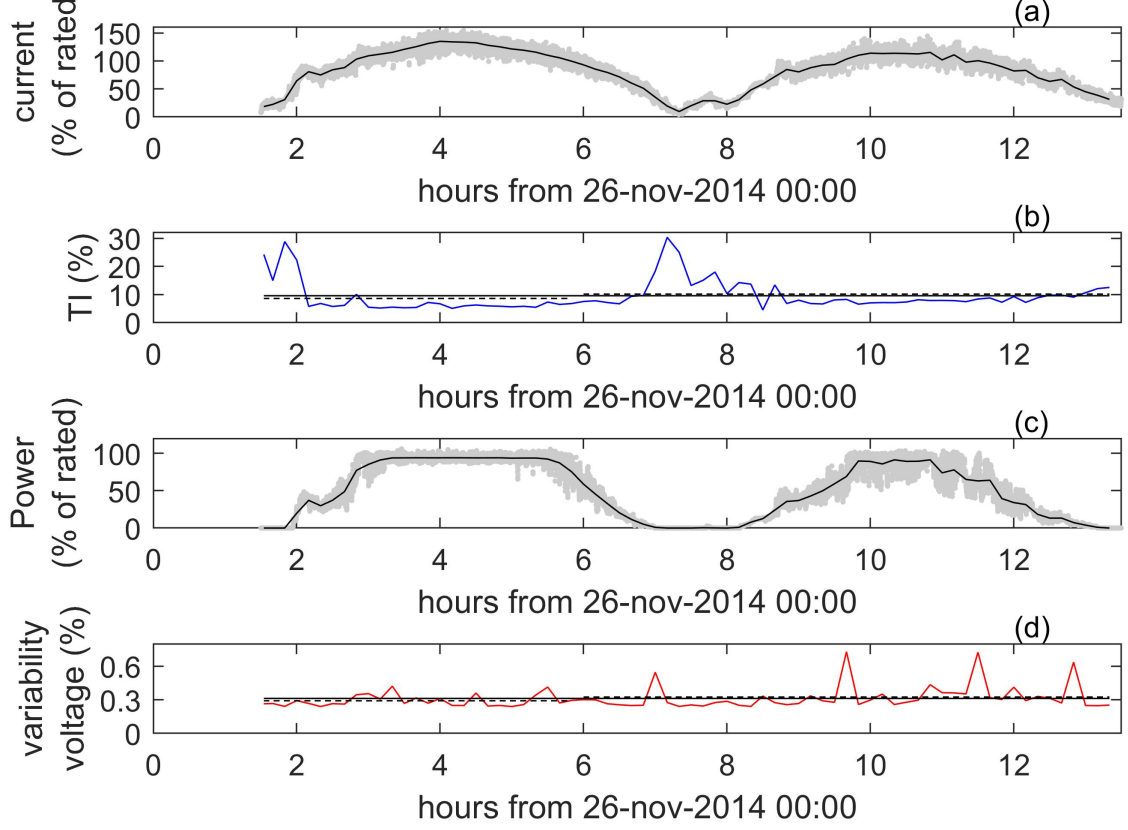
(a)
current (% of rated)
150
100
50
0
0
2
4
6
8
10
12
hours from 26-nov-2014 00:00
(b)
TI (%)
30
20
10
0
0
2
4
6
8
10
12
hours from 26-nov-2014 00:00
(c)
Power (% of rated)
100
50
0
0
2
4
6
8
10
12
hours from 26-nov-2014 00:00
(d)
variability voltage (%)
0.6
0.3
0
0
2
4
6
8
10
12
hours from 26-nov-2014 00:00

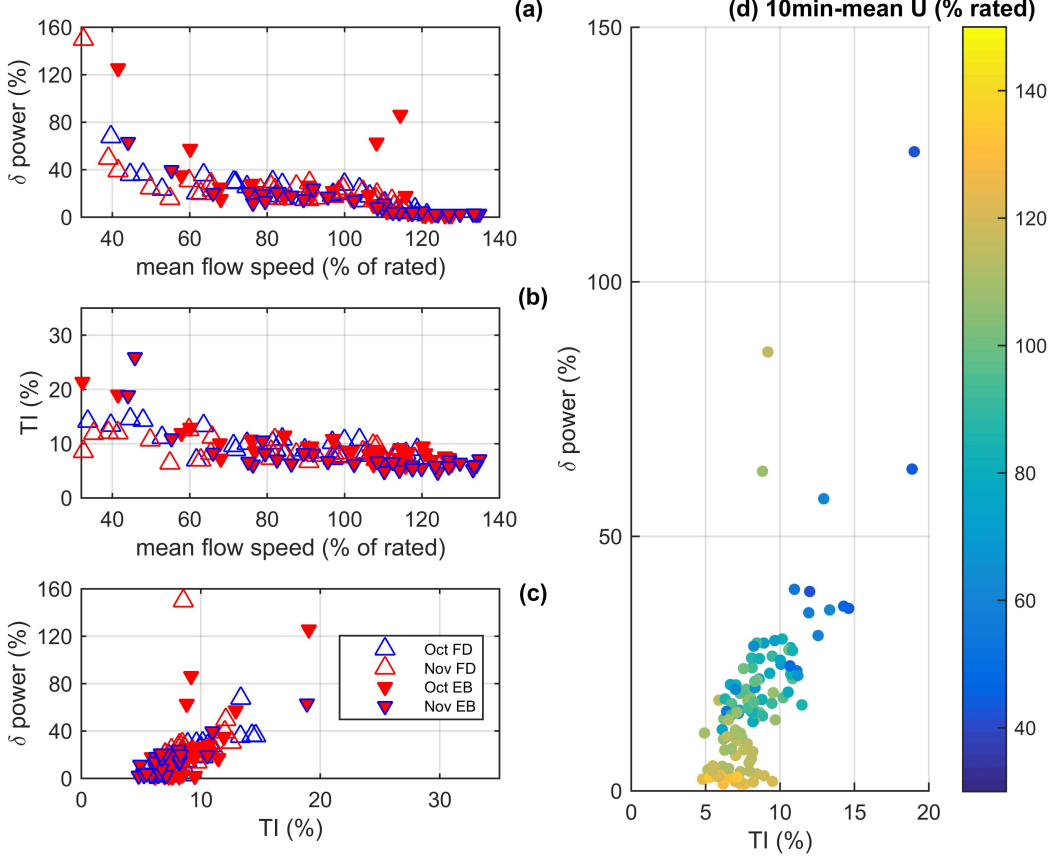
(a)
δ power (%)
mean flow speed (% of rated)
(b)
TI (%)
mean flow speed (% of rated)
(c)
δ power (%)
TI (%)
Oct FD
Nov FD
Oct EB
Nov EB
(d) 10min-mean U (% rated)
δ power (%)
TI (%)

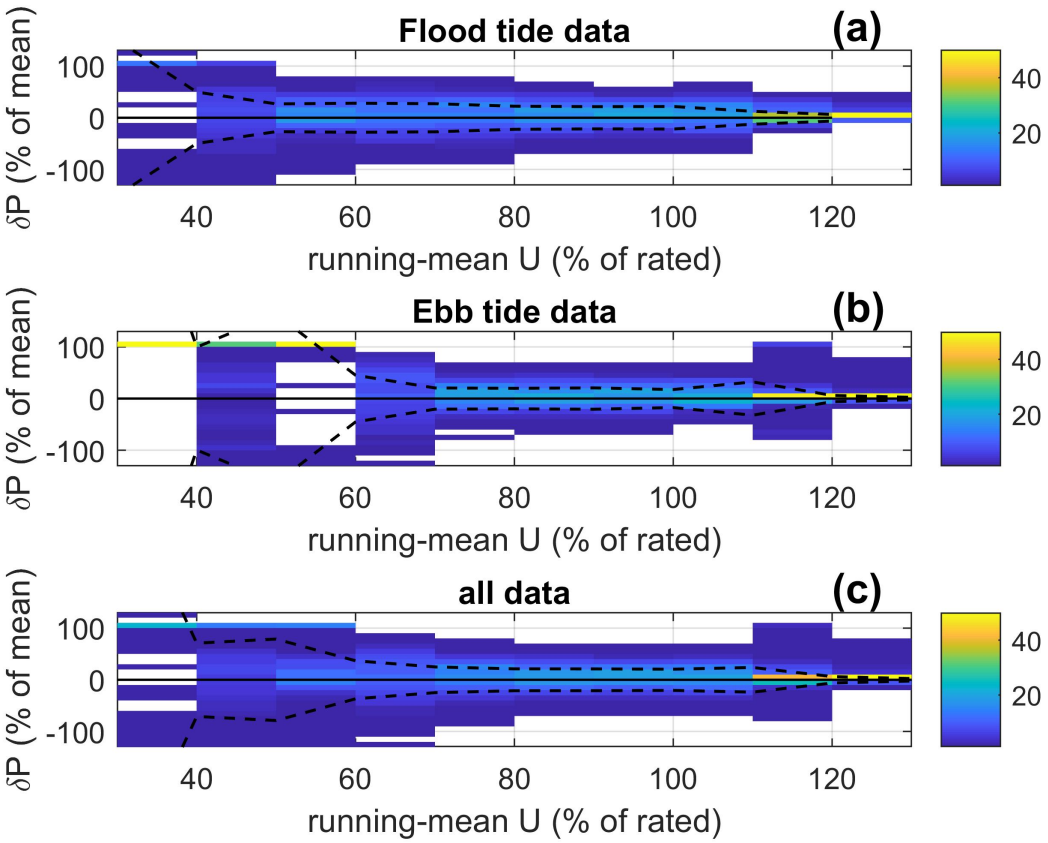
Flood tide data
(a)
100
0
-100
δP (% of mean)
40
60
80
100
120
running-mean U (% of rated)
40
20
Ebb tide data
(b)
100
0
-100
δP (% of mean)
40
60
80
100
120
running-mean U (% of rated)
40
20
all data
(c)
100
0
-100
δP (% of mean)
40
60
80
100
120
running-mean U (% of rated)
40
20

- Predictability and quality of tidal-stream energy may be undervalued at present